Simulation of liquid emptying from horizontal and inclined tubes with Smoothed Particle Hydrodynamics

Ana Cláudia Paulo Galhoz
ana.galhoz@ist.utl.pt

Instituto Superior Técnico, Lisboa, Portugal

November 2017

Abstract

Pipe emptying processes are commonly found in industry, related to applications in water supply, sewages, and hydro and nuclear plants. Unsteady free surface flows with large pressure variations can be observed in such processes. The application of the Smoothed Particle Hydrodynamics (SPH) method is proposed and applied, for the first time, to pipe emptying problems of an initially closed tube, in which one of its ends is suddenly opened and the liquid freely flows out from it. The SPH is a mesh free method and, due to its Lagrangian nature, is suitable to model the air cavity formed in the course of these motions. In order to study the influence of the pipe size and inclination angle on the physics process, a Matlab numerical implementation based on the incompressible Euler equations was considered. Several drift velocities were simulated and compared with theoretical values to assess the accuracy and stability of the simulations. The results showed good agreement with experimental and other simulated results available in the literature.

Keywords: inviscid fluid, incompressible flow, free surface, pipe emptying, Smooth Particle Hydrodynamics, numerical simulations

1 Introduction

Emptying of pipelines, involving interaction between air and water in pressurized systems, is widely used in hydraulic applications such as power stations, water-distribution networks, sewage systems, oil and gas industry, firefighting systems, and in pipeline cleaning and priming (see details in, e.g., [25, 26, 3]). During emptying procedures, air release valves or open standpipes allow the entrance of air into the hydraulic system, where air pockets may form (a thorough explanation can be found in [17]). In the course of these processes, many incidents like broken pumps, vales, and pipes, may occur due to unsteady fluid dynamics within the pipeline (more details on these phenomena in [18]). Therefore, it is of the most importance to develop knowledge of these piping systems, in order to prevent or at least minimize possible damages.

An *air cavity* may be formed by the emptying of an initially closed liquid-filled pipe. This phenomenon induces the motion of an air-liquid front through the pressurized pipeline, resulting in a pattern of sequences of long bubbles, followed by a liquid slug. The field of air cavities intrusions into circular pipes has been studied in hydraulic applications for a really long time as it can be confirmed in several articles, e.g., [36, 6, 1, 30, 7].

The problem of air cavity formation considered in this work was firstly introduced by Zukoski [36], in 1966, where an experimental study of the influence of surface tension, viscosity and pipe angle on the motion of air bubbles propagating upstream in an initially sealed circular pipe, by the sudden opening of one of the pipe's ends, was conducted. The results obtained were later on verified, in 1968, by Benjamin [6], when an analytical expression for the bubble velocity, denoted by *drift velocity*, for a horizontal circular pipe with neglected viscosity and surface tension was derived. Later, Alves *et al.* [1] extended Benjamin's analytical study to inclined and vertical cases, taking also into consideration surface tension effects.

For flows in slender pipes and channels, one-dimensional models are preferred due to the low computational effort and acceptable accuracy. The application or variants of Zukoski's experiment have been modelled in the one-dimensional space, e.g.,

by Tijsseling *et al.* in [28] and using an hydrostatic model in [5]. However, one-dimensional models cannot describe flow stratification, flow separation and fluid front evolution, which are phenomena encountered in this study. Therefore, two- and three-dimensional models are needed. Nevertheless, only two-dimensional problems are considered herein due to computational effort and analytical simplification.

In this work we are dealing with moving and deforming free boundaries which are hard to simulate with either Eulerian or Lagrangian grids. Therefore, we consider an approach based on moving "particles", i.e., instead of considering the fluid as a whole, we approximate it by a collection of particles. In particular, we consider the *Smoothed Particle Hydrodynamics* (SPH) numerical method, which is a proper choice because of its Lagrangian and mesh free features. In literature, due to its nature, it is very common to see applications of this method to free surface problems such as dam-breaks [23, 35, 16], impinging jet flows [29, 22] and others [10, 15, 20, 31].

The main goals of the present paper are the investigation of the air cavity intrusion into horizontal and inclined rectangular tubes, the numerical simulation of these pipe emptying problems by the *Incompressible Smoothed Particle Hydrodynamics* (ISPH) numerical method, and the analysis and comparison of the numerical results with theoretical, numerical and experimental results available in the literature.

In Sections 2 and 3, the mathematical modelling of the problem is presented, based on the Euler Equations for incompressible flow and on kinematic and dynamic boundary conditions at free surface. The methodology of the ISPH numerical method is introduced in Section 4 and, moreover, it is applied to the pipe emptying problems in Section 5. Section 6 is devoted to the numerical simulations, where several inclination angles and pipe dimensions are considered in order to study its effect on the rate of decrease of the liquid level through a dimensionless parameter, denominated by *Froude number* (or drift velocity), and the time of complete emptying of the pipeline. Later, in the same section, the numerical results are compared with theoretical, numerical and experimental results. The final conclusions are presented in Section 7.

2 Incompressible Euler Equations

In the present study, we deal with an incompressible inviscid flow. The deployed governing equations are the following (a detailed derivation of these equations can be found in, e.g., [2]):

$$\frac{\mathrm{D}\rho}{\mathrm{D}t} = 0, \tag{1}$$

$$\nabla \cdot \mathbf{v} = 0, \tag{2}$$

$$\frac{\mathrm{D}\mathbf{v}}{\mathrm{D}t} = \frac{-\nabla p}{\rho} + \mathbf{f}, \tag{3}$$

where ρ is the density, which is constant in time, p the pressure field, $\mathbf{v}$ the vector fluid velocity and $\mathbf{f}$ denotes the external forces. The momentum equation (3) is known as the *Euler equation*.

3 Problem Statement

Consider a variation of the Zukoski's [36] experiment, of an initially closed at both ends rectangular pipe and filled with water. One of these ends is suddenly open, and under the action of gravity, the liquid flows out freely from it. In the meantime, an air bubble propagates upstream along the tube towards the closed end, filling the previously occupied space by the ejected liquid.

The weight of the air bubble entering the cavity is taken to be negligible since it has much smaller density in comparison with the underlying fluid. Furthermore, since water is an almost incompressible fluid, the density changes very little, and one has the density of the system denoted by ρ. In addition, the viscosity, surface tension and energy loss are dismissed.

The surface represented by the air-water front is a free surface, and zero pressure is considered along it. Far upstream, the water fills the space of depth d and the velocity u_1 of the flow is constant; and, far downstream, the flow under the free boundary becomes uniform at depth h and velocity u_2.

A schematic description of the physical models of the two-dimensional pipe emptying problems for horizontal and inclined rectangular cavities in a fixed frame of reference is given in Figure 1.

Based on the latter assumptions and the incompressible Euler equations (1)-(3), the pipe emptying problems studied in this paper, within the domain $\Omega = \bigcup_{t\in[0,T]} \Omega(t) =]L(0), L(t)[\times]0, d(t)[$, with boundary $\partial\Omega = \bigcup_{t\in[0,T]} \partial\Omega(t) = \partial\Omega_w \cup \partial\Omega_f$ on the rigid walls in contact with the liquid and free surface, is described:

$$\begin{cases} \nabla \cdot \mathbf{v} = 0 & \text{in } \Omega \times [0,T], \\ \frac{\mathrm{D}\mathbf{v}}{\mathrm{D}t} = -\frac{\nabla p}{\rho} + \mathbf{g} & \text{in } \Omega \times [0,T], \\ \mathbf{v} \cdot \mathbf{n} = 0 & \text{on } \partial\Omega_w \times [0,T], \\ \mathbf{v}(\mathbf{x}, 0) = (0,0) & \forall \mathbf{x} \in \Omega(0), \end{cases} \tag{4}$$

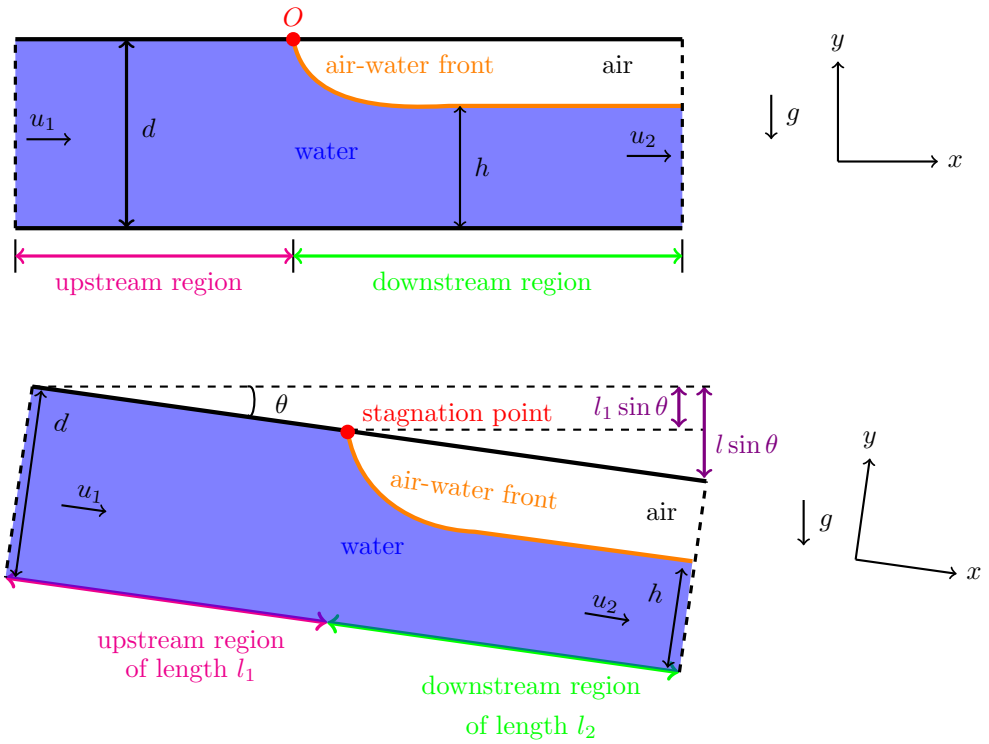

Figure 1: Two-dimensional steady flow past a horizontal (above) and an inclined cavity (below).

where the gravitational term $\mathbf{g} = (0, -g)$, or $\mathbf{g} = g(\sin\theta, -\cos\theta)$, for the horizontal and inclined cases, respectively; the domain parameters $L(0)$ and $L(t)$ represent the initial and at time t water-column lengths; $d(t)$ the height of the water-column at instant t; and $\mathbf{n}$ the surface normal.

The Dirichlet boundary condition is only applied on the top, bottom and left walls of the pipe in order to prevent the fluid of penetrating those walls.

In addition, the kinematic (5) and dynamic (6) conditions are considered along the free surface.

$$\frac{\mathrm{D}F}{\mathrm{D}t} = 0, \text{ for points } \mathbf{x}(t) = (l(t), d(t)) \quad (5)$$
$$\text{satisfying } F(\mathbf{x}, t) = 0,$$
$$p(\mathbf{x}, t) = 0, \text{ when } F(\mathbf{x}, t) = 0, \quad (6)$$

where F is a smooth function that defines the free surface.

4 ISPH method

First, we give a summary of the SPH methodology.

The value of a continuous scalar field $f : \Omega \subset \mathbb{R}^2 \to \mathbb{R}$ at an arbitrary point $\mathbf{x} = (x_1, x_2) \in \Omega$ can be given by:

$$f(\mathbf{x}) = \int_\Omega f(\mathbf{x}')\delta(\mathbf{x} - \mathbf{x}')\mathrm{d}\mathbf{x}', \quad (7)$$

where $\delta(.)$ is the *Dirac delta distribution*. In the SPH scheme, $\delta(\mathbf{x} - \mathbf{x}')$ is replaced with an approximation (details of this argument in [19]), denominated by *smoothing* or *kernel function* $W(\mathbf{x}-\mathbf{x}', h)$, with $h > 0$ *smoothing parameter* which defines the influence area of the smoothing function W. These kernel functions should be positive, radial symmetric, monotonic, have compact support and other characteristics, which can be consulted with detail in [21].

In this paper, the *Wendland kernel function* [32] is considered:

$$W(R, h) = \frac{\lambda}{h^2} \begin{cases} (1 - \frac{1}{2}R)^\alpha (\frac{\alpha}{2}R + 1) & \text{if } 0 \le R < 2, \\ 0, & \text{otherwise,} \end{cases} \quad (8)$$

where $\alpha = 4$, $\lambda = \frac{7}{4\pi}$ and $R = \dfrac{r}{h} = \dfrac{\|\mathbf{x} - \mathbf{x}'\|}{h}$.

Denote $\mathcal{L}^0 f()$ as the approximation operator of the function $f()$. In addition, the approximation of β-th order derivative operators $D^\beta f()$ will be denoted by $\mathcal{L}^\beta f()$. Hence, the approximated *kernel representation* of $f(\mathbf{x})$ is given by

$$\mathcal{L}^0 f(\mathbf{x}) = \int_\Omega f(\mathbf{x}')W(\mathbf{x} - \mathbf{x}', h)d\mathbf{x}'. \quad (9)$$

Furthermore, approximating (9) by a spatial discretization using scattered particles, yields the *par-*

ticle approximation expression:

$$\mathcal{L}^0 f(\mathbf{x}) = \sum_{j=1}^{N} f(\mathbf{x}_j) W(\mathbf{x} - \mathbf{x}_j, h) \Delta V_j, \qquad (10)$$

where ΔV_j is the finite volume of the particle j and N denotes the number of particles in the neighbourhood of $\mathbf{x}$.

In accordance, the particle approximation for a function at particle i can be defined

$$\mathcal{L}^0 f_i = \sum_{j=1}^{N} \frac{m_j}{\rho_j} f(\mathbf{x}_j).W_{ij}, \qquad (11)$$

with f_i denoting $f(\mathbf{x}_i)$, $m_j = \Delta V_j \rho_j$, where m_j and ρ_j represent the mass and density of particle j, respectively, and

$$W_{ij} = W(\mathbf{x}_i - \mathbf{x}_j, h) = W(\|\mathbf{x}_i - \mathbf{x}_j\|, h) = W(R_{ij}, h), \qquad (12)$$

with $R_{ij} = \frac{r_{ij}}{h} = \frac{\|\mathbf{x}_i - \mathbf{x}_j\|}{h}$ being the relative distance between particles i and j.

The particle approximation of the gradient for a scalar field f at particle i can be written as

$$\mathcal{L}^1 f(\mathbf{x}_i) = \sum_{j=1}^{N} \frac{m_j}{\rho_j} f(\mathbf{x}_j) \cdot \nabla_i W_{ij}, \qquad (13)$$

with

$$\nabla_i W_{ij} = \frac{\mathbf{x}_i - \mathbf{x}_j}{r_{ij}} \frac{\partial W_{ij}}{\partial r_{ij}} = \frac{\mathbf{x}_{ij}}{r_{ij}} \frac{\partial W_{ij}}{\partial r_{ij}}. \qquad (14)$$

Although the gradient particle approximation is expressed by (13), several variants of SPH formulations have been developed in literature (see, e.g., [19, 21]). Two of them are listed below:

$$\mathcal{L}^1 f(\mathbf{x}_i) = \sum_{j=1}^{N} \frac{m_j}{\rho_j} \big(f(\mathbf{x}_j) - f(\mathbf{x}_i)\big) \cdot \nabla_i W_{ij}, \quad (15)$$

$$\mathcal{L}^1 \mathbf{f}(\mathbf{x}_i) = -\sum_{j=1}^{N} \frac{m_j}{\rho_j} \big(\mathbf{f}(\mathbf{x}_i) - \mathbf{f}(\mathbf{x}_j)\big) \cdot \nabla_i W_{ij}, \quad (16)$$

where (15) and (16) approximate a scalar field and a vector field, respectively.

To approximate the Laplacian of a scalar field f, we consider the following approximation proposed by Brookshaw in [8]:

$$\mathcal{L}^2 f(\mathbf{x}_i) = 2 \sum_{j=1}^{N} \frac{m_j}{\rho_j} \big(f(\mathbf{x}_i) - f(\mathbf{x}_j)\big) \frac{\mathbf{r}_{ij} \cdot \nabla_i W_{ij}}{||\mathbf{r}_{ij}||^2}. \qquad (17)$$

Since the classic SPH method is originally developed for compressible flows, some special treatment for the incompressible condition is required. Hence, for this study, the ISPH method based on a projection method, which calculates the pressure field by computation of a discretized *pressure Poisson equation* (PPE), is employed.

In the following equations, the superscripts n and n + 1 denote the current and next time step, respectively. The Explicit-Implicit Predictor-Corrector projection method, presented in [11], includes several steps. For the first predictor step, auxiliary velocities without pressure gradient are considered,

$$\mathbf{v}_i^* = \mathbf{v}_i^n + \mathbf{g}\Delta t. \qquad (18)$$

Then, the following corrector step introduces an effect of "next" pressure, based on the Euler equations (1)-(3), as follows:

$$\mathbf{v}_i^{n+1} = \mathbf{v}_i^* + \Delta t \bigg(-\frac{1}{\rho} \nabla p_i^{n+1} \bigg). \qquad (19)$$

In order to ensure a divergence-free velocity field, we re-arrange the terms and apply the divergence on both sides of (19),

$$\nabla \cdot \left(\frac{\mathbf{v}_i^{n+1} - \mathbf{v}_i^*}{\Delta t} \right) = \nabla \cdot \bigg(-\frac{1}{\rho} \nabla p_i^{n+1} \bigg). \qquad (20)$$

Then, the incompressible condition (2) leads to

$$\nabla \cdot \mathbf{v}_i^{n+1} = 0. \qquad (21)$$

Since ρ is constant and substituting (21) into (20), the following pressure Poisson equation is obtained:

$$\frac{\rho}{\Delta t} \big(\nabla \cdot \mathbf{v}_i^*\big) = \nabla^2 p_i^{n+1}. \qquad (22)$$

Then, the velocity field at time step $n + 1$ can be computed by substituting the pressure gradient with the solution of the latter PPE.

5 Application of ISPH

Bearing in mind the ISPH scheme introduced in the previous section, we have as the first step of the simulation, the computation of the auxiliary velocity:

$$\mathbf{v}_i^* = \mathbf{v}_i^n + \mathbf{g}_i \Delta t, \qquad (23)$$

where the vector of gravitational acceleration $\mathbf{g}_i \equiv \mathbf{g} = (0, -g)$ for the horizontal pipe emptying problem and $\mathbf{g} = g(\sin\theta, -\cos\theta)$ for the inclined one.

Moreover, to calculate the pressure field p, the left-hand side of (22) is computed by substitution of the vector field $\mathbf{f}$ in (16) with the auxiliary velocity field $\mathbf{v}^*$, which yields:

$$\nabla \cdot \mathbf{v}^*(\mathbf{x}_i) = -\sum_{j=1}^{N} (\mathbf{v}^*(\mathbf{x}_i) - \mathbf{v}^*(\mathbf{x}_j)) \cdot \nabla_i W_{ij} \Delta V_j. \qquad (24)$$

Then, to deal with the right-hand side of (22), the SPH formulation (17) is taken, which results in the following expression for the pressure Laplacian:

$$\nabla^2 p_i = 2\sum_{j=1}^{N}\left(p_i - p_j\right)\frac{\mathbf{r}_{ij}\cdot\nabla_i W_{ij}}{||\mathbf{r}_{ij}||^2}\Delta V_j. \tag{25}$$

In order to complete the computation of the PPE (22), the following boundary conditions for the pressure are prescribed:

$$p_{i,m} = p_i, \tag{26}$$

$$p_{front} = 0, \tag{27}$$

where $p_{i,m}$ is the pressure of the mirrored particle and p_{front} represents the pressure of a free surface particle at the front of the air-water cavity in Figure 1. This mirror particle concept comes as result of the application of the boundary treatment sheme, denominated *mirror particles* introduced in [24].

Next, the accelerations given by the momentum equation without the gravity force,

$$\frac{\mathrm{D}\mathbf{v}}{\mathrm{D}t} = \frac{-\nabla p}{\rho}, \tag{28}$$

are calculated using the SPH formulation (15) with the addition of a correction term $\mathbf{\Gamma}^{-1}_{i,\nabla}$ as introduced by Chen *et al* in [9], as follows:

$$\frac{\mathrm{D}\mathbf{v}_i}{\mathrm{D}t} = -\mathbf{\Gamma}^{-1}_{i,\nabla}\sum_{j=1}^{N}\left(\frac{p_j^{n+1} - p_i^{n+1}}{\rho}\right)\nabla_i W_{ij}\Delta V_j. \tag{29}$$

5.1 Update particle velocities and positions

For the simulations displayed in the next section, initial conditions for the positions and velocities of the particles are required. Regarding the positions, for both horizontal and inclined cases, the particles are distributed within an hexagonal distribution since it is more stable than a random or uniform lattice (details of this argument in [12]).

In order to solve (29) and update the particles positions, we consider the *Euler forward method* since it is the most straightforward, as well as the cheapest in data storage scheme. Thus, it follows:

$$\mathbf{v}_i^{n+1} = \mathbf{v}_i^n + \left(\frac{\mathrm{D}\mathbf{v}_i}{\mathrm{D}t}\right)^{n+1}\Delta t. \tag{30}$$

Then, it is possible to move the particles and update their new positions according to the following expression:

$$\mathbf{x}_i^{n+1} = \mathbf{x}_i^n + \mathbf{v}_i^{n+1}\Delta t. \tag{31}$$

Note that in the expressions (30) and (31) the time step Δt is evaluated according to the *Courant-Friedrichs-Lewy* (CFL) condition for stability (see [27]),

$$\Delta t \leq \lambda\frac{\Delta x_0}{c}, \tag{32}$$

where $\lambda = \eta C_{CFL}/(1+Ma)$.
For this work, a low Mach number $Ma = 0.1$, $\eta = 1.5$ and C_{CFL} such that $\lambda \approx 1$ are assumed. In addition, the artificial speed of sound c is chosen to satisfy $c = V_{max}/Ma$, where the maximum velocity is acquired by the analytical maximum Froude number deduced by Benjamin in [6] for a two-dimensional pipe emptying problem with energy loss, with the value $V_{max} = 0.5273\sqrt{gd}$.

6 Results and discussion

Simulations in Matlab were carried out with fluid density $\rho = 1000$ kg/m^3, gravitational acceleration $g = 9.8$ m/s^2 and smoothing length $h = 1.5dx$ or $h = 1.2dx$ (dx is the initial particle distance in the x-direction), for the horizontal and inclined cases, respectively, for several pipe widths d, lengths L and inclination angles θ.

In this section we are interested in understanding how variations on the parameters referred above, affect the pipe emptying time and the Froude number. This last one is of the most importance since gives information about how the gravitational and inertial forces are related (see a more detailed description in [4]) and, therefore, is directly related with the stability and accuracy of the pipe emptying process. In order to validate our results, theoretical expressions of the drift velocity are derived based on Bernoulli's equation (see [33]) and conservation of mass, applied for the simulations and compared with theoretical values.

6.1 Horizontal pipe

For the horizontal pipe emptying problem, simulations for length-diameter ratios 20:1 to 60:1 were performed. For each ratio, two examples are presented, where in the first one a bigger pipe is taken into consideration. Furthermore, for each one of the examples, the same (or at least approximated) number of particles N_{total} is taken in order to make a suitable future analysis of these simulation parameters on the pipe emptying process.

In Figure 2, an illustration of the horizontal pipe emptying process for a length-diameter ratio 40:1, can be observed.

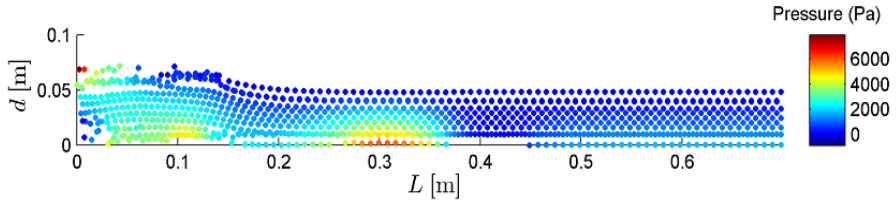

(a)

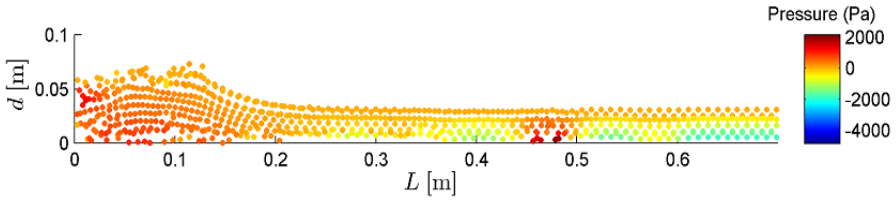

(b)

Figure 2: Horizontal pipe emptying process for a length-diameter ratio 40:1, Example I. (a) At $t = 0.105$ s. (b) At $t = 0.15$ s.

First, we analyse the time it takes to empty the horizontal pipe and present the results in Table 1.

Next, we study the drift velocities. A schematic description of the physical models of the two-dimensional pipe emptying problems for horizontal and inclined rectangular cavities in a frame of reference travelling with the front of the cavity, which enables the motion of the water to appear steady, is given in Figure 1.

Table 1: Pipe emptying time for length-diameter ratios 20:1 to 60:1.

	Time-emptying (s)
Ratio 20:1	
Example I	0.8220
Example II	0.4220
Ratio 30:1	
Example I	0.6480
Example II	0.3350
Ratio 40:1	
Example I	0.5775
Example II	0.2910
Ratio 50:1	
Example I	0.4665
Example II	0.3030
Ratio 60:1	
Example I	0.5085
Example II	0.2120

Hence, by consideration of the horizontal cavity illustration and performing an analytical study, an expression for the Froude number in the far upstream section is obtained:

$$Fr_1 = \frac{u_1}{\sqrt{gd}}, \tag{33}$$

where

$$u_1 = u_2 \frac{h}{d} \tag{34}$$

$$u_2^2 = 2g(d - h). \tag{35}$$

Table 2: Froude numbers for length-diameter ratios 20:1 to 60:1.

	Froude number Fr_1
Ratio 20:1	
Example I	0.5436
Example II	0.5303
Ratio 30:1	
Example I	0.5051
Example II	0.4480
Ratio 40:1	
Example I	0.4558
Example II	0.4717
Ratio 50:1	
Example I	0.4493
Example II	0.3293
Ratio 60:1	
Example I	0.2246
Example II	0.3953

This yields the expression:

$$Fr_1 = \frac{\sqrt{2(d-h)}h/d}{\sqrt{d}}. \tag{36}$$

Based on equation (36), and considering the value of the water-column h for each one of the simulations, the Froude number of the far upstream region for each one of the simulations is calculated and presented in Table 2.

In the literature it is possible to find results based on other simulation methods and experiments for the horizontal pipe emptying problem. These results are presented in the following Table 3.

Table 3: Theoretical, experimental and simulated Froude numbers for length-diameter ratio 60:1.

	Froude number Fr_1
Theoretical	
Benjamin [6]	0.5000
Experimental	
Gardner and Crown [14]	0.4900
Wilkinson [34]	0.4800
Simulated	
VOF Model	
Anderson [2]	0.4550
VOF Model	
Anderson [2]	0.4440
Hydrostatic Model	
Bashiri-Atrabi [5]	0.5254
Boussinesq Model	
Bashiri-Atrabi [5]	0.5095

6.2 Inclined pipe

Similarly to the previous section, we pretend to evaluate the pipe inclination angle θ on the pipe's emptying time and drift velocity. Therefore, we take the same (or at least approximated) number of particles N_{total} and $\theta = 8°, 30°, 45°, 80°$.

For these simulations, we consider a reference frame with the axis $\mathbf{e_x}$ aligned with the tube, i.e., rotated by the same angle of inclination of the tube. As a consequence, the fluid domain will be represented as a horizontal region and the gravity vector will be composed into two components $\mathbf{g} = g(\sin\theta, -\cos\theta)$ instead of being represented along the vertical direction only.

In Figure 3, an illustration of the inclined pipe emptying process for a downward slope of $\theta = 8°$, can be observed.

The time it takes to empty an inclined pipe is presented in Table 4.

Table 4: Pipe emptying time for inclination angles $\theta = 8°, 30°, 45°, 80°$.

	Time-emptying (s)
Angle $\theta = 8°$	0.2140
Angle $\theta = 30°$	~ 0.1796
Angle $\theta = 45°$	~ 0.1499
Angle $\theta = 80°$	~ 0.1420

Moreover, bearing in mind the inclined cavity illustration in Figure 1 and assuming an analytical study, the Froude number expression in the far upstream region is achieved:

$$Fr_1 = \frac{u_1}{\sqrt{g(d\cos\theta)}}, \tag{37}$$

where

$$u_1 = u_2 \frac{\big(h\cos\theta + l\sin\theta\big)}{d\cos\theta} \tag{38}$$

$$u_2^2 = 2g\big((d-h)\cos\theta - l_2\sin\theta\big). \tag{39}$$

This results in the following expression:

$$Fr_1 = \frac{\sqrt{2(d-h)\cos\theta - l_2\sin\theta}\big(h\cos\theta + l\sin\theta\big)}{(d\cos\theta)^{1+1/2}}. \tag{40}$$

Based on the equation (40), and considering the value of the water-column h for each one of the simulations, the Froude number of the far upstream region for each one of the simulations is calculated and presented in Table 5.

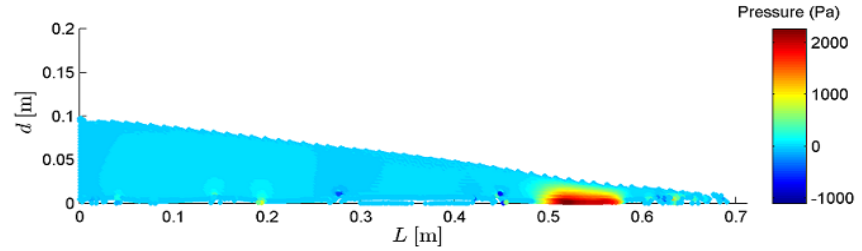

(a)

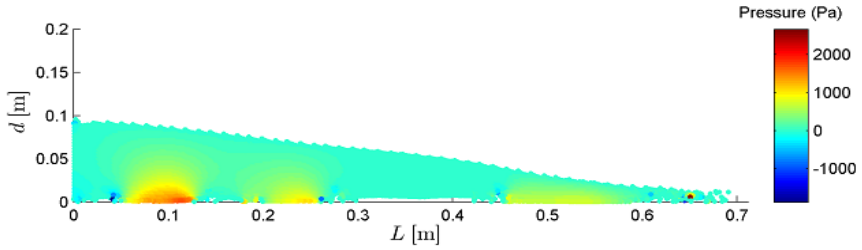

(b)

Figure 3: Inclined pipe emptying process for a downward slope of $\theta = 8°$. (a) At $t = 0.0524$ s. (b) At $t = 0.0608$ s.

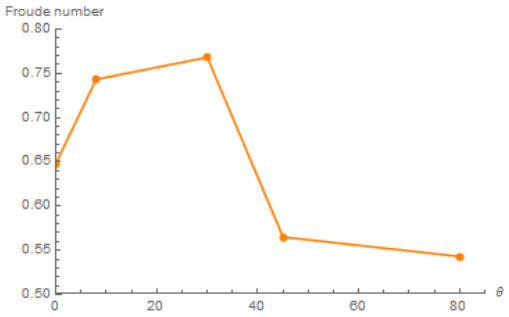

Figure 4: Variation of Froude number Fr_{t_1} with inclination angle θ.

Table 5: Froude numbers for inclination angles $\theta = 8°, 30°, 45°, 80°$.

	Froude number Fr_1
Angle $\theta = 8°$	0.7434
Angle $\theta = 30°$	0.7682
Angle $\theta = 45°$	0.5651
Angle $\theta = 80°$	0.5431

In the literature it is possible to find results based on other simulation methods and experiments for the inclined pipe emptying problem. These results are presented in the following Table 6.

Table 6: Theoretical, experimental and simulated Froude numbers for several inclination angles θ.

	Froude number Fr_1
Theoretical	
Dumitrescu [13], $\theta = 90°$	0.3520
Experimental	
Dumitrescu [13], $\theta = 90°$	0.3460
Zukoski [36], $\theta = 90°$	0.3400
Zukoski [36], $\theta = 45°$	0.4300
Zukoski [36], $\theta = 8°$	0.3200
Simulated	
VOF Model	
Anderson [2], $\theta = 90°$	0.4520
VOF Model	
Anderson [2], $\theta = 90°$	0.3970
Hydrostatic Model	
Bashiri-Atrabi [5], $\theta = 8°$	0.6913
Boussinesq Model	
Bashiri-Atrabi [5], $\theta = 8°$	0.8201

7 Conclusions

In this paper we introduced the mesh-free Lagrangian particle based method Smoothed Particle Hydrodynamics (SPH) to the two-dimensional pipe emptying problems of initially closed horizontal and inclined tubes in which one of the ends is suddenly open, analysed by Zukoski in [36]. The aim of this work was to study the influence of the pipe size and inclination angle on the physics of the emptying process through the dimensionless Froude number, and compare the results obtained with theoretical, experimental and other simulated results found in literature.

The following conclusions can thus be drawn from this study:

- Regarding the inclined pipe emptying problem, we noticed that for higher inclination angles, the range of pressure distribution values would also increase;
- Considering the Froude numbers for the horizontal and inclined cases, we define that the drift velocity increases from the vertical position until an intermediate value of θ. From which it starts to decrease again until the horizontal position, where the lowest drift velocity was encountered. This phenomenon had been already described in several articles from literature for some experimental works;
- The simulated Froude numbers, for non-zero slopes, were not close to the experimental values. Although, they were close to other simulated ones for an inclination angle of $\theta = 8°$;
- Concerning the time it takes to empty the pipe, we deducted that for smaller tubes and bigger inclination angles, it would take significantly less time to achieve this.

Overall, we conclude that the performance of the SPH method to these pipe emptying problems delivered good results which where mostly validated by theoretical, experimental and other simulated results.

7.1 Future work

As it was just mentioned, we obtained satisfactory results with the application of the SPH Lagrangian method. However, the reader should note that these outcomes were achieved based on simplified conditions. For more realistic results, we indicate the consideration of a circular pipe, i.e., a three-dimensional problem, viscosity and surface tension, and energy loss.

References

[1] I. N. Alves, O. Shoham, and Y. Taitel. Drift velocity of elongated bubbles in inclined pipes. *Chemical engineering science*, 48(17):3063–3070, 1993.

[2] J. D. Anderson. *Computational Fluid Dynamics: The Basics with Applications*. McGraw-Hill, 1995.

[3] A. Bahadori. *Oil and gas pipelines and piping systems: design, construction, management, and inspection*. Gulf Professional Publishing, 2016.

[4] R. Bansal. *A Text Book of Fluid Mechanics and Hydraulic Machines: In MKS and SI Units*. Laxmi publications, 1989.

[5] H. Bashiri-Atrabi, T. Hosoda, and H. Shirai. Propagation of an air-water interface from pressurized to free-surface flow in a circular pipe. *Journal of Hydraulic Engineering*, 142(12):04016055, 2016.

[6] T. B. Benjamin. Gravity currents and related phenomena. *Journal of Fluid Mechanics*, 31(2):209–248, 1968.

[7] S. Bousso and M. Fuamba. Numerical and experimental analysis of the pressurized wave front in a circular pipe. *Journal of Hydraulic Engineering*, 140(3):300–312, 2013.

[8] L. Brookshaw. A method of calculating radiative heat diffusion in particle simulations. *Publications of the Astronomical Society of Australia*, 6(2):207–210, 1985.

[9] J. Chen, J. Beraun, and T. Carney. A corrective smoothed particle method for boundary value problems in heat conduction. *International Journal for Numerical Methods in Engineering*, 46(2):231–252, 1999.

[10] A. Colagrossi, M. Antuono, and D. Le Touzé. Theoretical considerations on the free-surface role in the smoothed-particle-hydrodynamics model. *Physical Review E*, 79(5):056701, 2009.

[11] S. J. Cummins and M. Rudman. An SPH projection method. *Journal of computational physics*, 152(2):584–607, 1999.

[12] S. Diehl, G. Rockefeller, C. L. Fryer, D. Riethmiller, and T. S. Statler. Generating optimal initial conditions for smoothed particle hydrodynamics simulations. *Publications of the Astronomical Society of Australia*, 32, 2015.

[13] D. T. Dumitrescu. Strömung an einer luftblase im senkrechten rohr. *ZAMM-Journal of Applied Mathematics and Mechanics/Zeitschrift für Angewandte Mathematik und Mechanik*, 23(3):139–149, 1943.

[14] G. Gardner and I. Crow. The motion of large bubbles in horizontal channels. *Journal of Fluid Mechanics*, 43(2):247–255, 1970.

[15] Q. Hou, L. Zhang, A. Tijsseling, and A. Kruisbrink. Rapid filling of pipelines with the SPH particle method. *Procedia Engineering*, 31:38–43, 2012.

[16] W. Jian, D. Liang, S. Shao, R. Chen, K. Yang, et al. Smoothed particle hydrodynamics simulations of dam-break flows around movable structures. *International Journal of Offshore and Polar Engineering*, 26(01):33–40, 2016.

[17] J. Laanearu, I. Annus, T. Koppel, A. Bergant, S. Vučković, Q. Hou, A. S. Tijsseling, A. Anderson, and J. M. vant Westende. Emptying of large-scale pipeline by pressurized air. *Journal of Hydraulic Engineering*, 138(12):1090–1100, 2012.

[18] D. Leslie and A. Vardy. Practical guidelines for fluid-structure interaction in pipelines: a review. In *Proc. of the 10th international meeting of the work group on the behaviour of hydraulic machinery under steady oscillatory conditions*, 2001.

[19] S. Li and W. K. Liu. *Meshfree Particle Methods*. Springer Science & Business Media, 2007.

[20] S. Lind, R. Xu, P. Stansby, and B. D. Rogers. Incompressible smoothed particle hydrodynamics for free-surface flows: A generalised diffusion-based algorithm for stability and validations for impulsive flows and propagating waves. *Journal of Computational Physics*, 231(4):1499–1523, 2012.

[21] G.-R. Liu and M. B. Liu. *Smoothed particle hydrodynamics: a meshfree particle method*. World Scientific, 2003.

[22] J.-C. Marongiu, F. Leboeuf, J. Caro, and E. Parkinson. Free surface flows simulations in pelton turbines using an hybrid SPH-ALE method. *Journal of Hydraulic Research*, 48(S1):40–49, 2010.

[23] J. J. Monaghan. Simulating free surface flows with SPH. *Journal of computational physics*, 110(2):399–406, 1994.

[24] J. P. Morris, P. J. Fox, and Y. Zhu. Modeling low reynolds number incompressible flows using SPH. *Journal of computational physics*, 136(1):214–226, 1997.

[25] D. B. Rushmore. *Hydro-electric power stations.* , 1923.

[26] C. Suribabu. Location and sizing of scour valves in water distribution network. *ISH Journal of Hydraulic Engineering*, 15(2):118–130, 2009.

[27] J. W. Thomas. *Numerical partial differential equations: finite difference methods*, volume 22. Springer Science & Business Media, 2013.

[28] A. S. Tijsseling, Q. Hou, Z. Bozkuş, and J. Laanearu. Improved one-dimensional models for rapid emptying and filling of pipelines. *Journal of Pressure Vessel Technology*, 138(3):031301, 2016.

[29] M. F. Tome and S. Mckee. Numerical simulation of viscous flow: buckling of planar jets. *International journal for numerical methods in fluids*, 29(6):705–718, 1999.

[30] J. G. Vasconcelos and S. J. Wright. Rapid flow startup in filled horizontal pipelines. *Journal of Hydraulic Engineering*, 134(7):984–992, 2008.

[31] D. Violeau and B. D. Rogers. Smoothed particle hydrodynamics (SPH) for free-surface flows: past, present and future. *Journal of Hydraulic Research*, 54(1):1–26, 2016.

[32] H. Wendland. Piecewise polynomial, positive definite and compactly supported radial functions of minimal degree. *Advances in computational Mathematics*, 4(1):389–396, 1995.

[33] F. M. White. *Fluid Mechanics, 7^{th} edition.* McGraw-Hill, 2011.

[34] D. Wilkinson. Motion of air cavities in long horizontal ducts. *Journal of Fluid Mechanics*, 118:109–122, 1982.

[35] X. Zheng and W.-y. Duan. Numerical simulation of dam breaking using smoothed particle hydrodynamics and viscosity behavior. *Journal of Marine Science and Application*, 9(1):34–41, 2010.

[36] E. Zukoski. Influence of viscosity, surface tension, and inclination angle on motion of long bubbles in closed tubes. *Journal of Fluid Mechanics*, 25(4):821–837, 1966.